

DESIGN AND EXPERIMENT OF A MOREL PICKING MACHINE

羊肚菌采摘机设计与试验

Xiaohu BAI, Xiang ZOU, Zexu WANG, Guojing DU, Chuan LI, Chonghe GAO

College of Engineering, Shenyang Agricultural University, Shenyang/China

E-mail: baixiaohu@syau.edu.cn

DOI: <https://doi.org/10.35633/inmateh-75-36>**Keywords:** *Robotic arm, Picking claw, Blade length, Simulation, Morel***ABSTRACT**

To address the challenges of high labour intensity and expensive manpower in morel harvesting, a specialized morel picking machine was designed. It is capable of performing the tasks of grasping, cutting, and collecting morels. A three-degree-of-freedom robotic arm was incorporated to ensure precise positioning of the picking claw. The kinematic model of this arm was established to determine the operational radius for effective picking. A three-finger picking claw was developed, with the synchronous opening and closing of the three fingers through a wire-pulling mechanism and a four-bar linkage. Buffer elastic material was installed on the picking fingers, and cutting blades were placed at the fingertips. Simulation analyses were conducted to study the movement of the robotic arm's end, the forces acted on the picking arm, the hinge between the upper and lower arms, and the hinge at the lower arm's end, as well as the velocity of the picking claw's end. Single-factor experiments were employed to investigate the effects of the blade length of the picking finger on the picking success rate, the damage rate of mature morels, and the damage rate of immature morels. The results demonstrated that with a blade length set at 15mm, the picking success rate reached 96.2%, while the damage rates of mature and immature morels were 8.6% and 6.8%, respectively. These findings indicate that the machine can effectively meet the operational requirements for morel picking.

摘要

为解决羊肚菌采摘劳动强度大、人工成本高的问题,设计了一种羊肚菌采摘机,可以完成抓取、切断、收集作业。采用三自由度机械臂实现采摘爪的精确定位,建立了机械臂的运动学模型,确定了采摘作业半径。设计了三指结构采摘爪,通过拉线驱动与四杆机构实现三指同时闭合和松开。采摘手指上安装缓冲弹性材料,末端装有切割刀片。对机械臂末端运动、机械臂受力、大臂与小臂铰链处作用力、小臂末端铰链处作用力、采摘爪末端速度进行了仿真分析。通过单因素试验,研究了采摘手指刀片长度对采摘成功率、羊肚菌损伤率、未成熟羊肚菌损伤率的影响。结果表明,当刀片长度为15mm时,采摘成功率为96.2%,采摘损伤率为8.6%,未成熟羊肚菌损伤率为6.8%,基本满足羊肚菌采摘的作业要求。

INTRODUCTION

Morel mushrooms are rich in nutrients and trace elements, and are widely cultivated in China (Huang *et al.*, 2022; Liu *et al.*, 2017; Zhao *et al.*, 2009). Due to the unique growth environment of morels, their fragile texture, and significant variations in individual morphology, traditional manual harvesting methods are labour-intensive and inefficient (Huang *et al.*, 2023). As labour costs rise and the demand for high-quality picking increases, developing equipment that is suitable for the characteristics of morels is crucial for enhancing the economic benefits of the morel industry and increasing farmers' incomes.

Currently, numerous studies focus on the end effectors and grasping mechanisms of fruit and vegetable picking machinery; however, there are relatively few reports on morel picking machinery (Li *et al.*, 2014; Safeea *et al.*, 2019; Wang *et al.*, 2016; Gu *et al.*, 2012; Ding *et al.*, 2013). Yang developed a mushroom picking machine that achieved autonomous movement and stopping through a mobile platform. This machine collected mushroom data using a visual system and controlled the actuator to pick and load the mushrooms (Yang, 2020). Zhang investigated a portabella picking robot, which features a mobile lifting platform, adjustable guide rails, picking arms, flexible picking claws, as well as a visual recognition and positioning system, along with a measurement and control system (Zhang, 2019). Wang studied a morel harvesting machine that consists of a storage box, an air tube, a cutting device, and a blower fan. After the stem of the morel is cut off, it is sucked into the box.

Although the machine has a simple structure and high picking efficiency, it is prone to damaging the morels, and the fan consumes a significant amount of energy (Wang *et al.*, 2021). Wang developed a morel harvesting device that includes a sleeve and two blades. Through the interaction of the blades, the morels can be extracted from the soil, while the soil attached to the morels is expelled through holes in the blades (Wang, 2021). Yu designed a morel harvesting tool featuring scissors mounted on a support frame. The scissors are operated by an electric push rod, and a conveyor belt transports the morels into a receiving bucket (Yu, 2022). Additionally, Wang created a morel picking device equipped with a cylindrical component and a blade, with the blade affixed to the bottom of the cylindrical component and operated by a handle (Wang, 2019).

In this paper, to address the challenges of high labour intensity, susceptibility to damage, and high labour costs associated with morel harvesting, a morel picking machine that performs the functions of grasping, cutting, and collecting morels was designed. This machine not only ensures efficient harvesting operations but also effectively minimizes damage to the morels.

MATERIALS AND METHODS

Structure of the machine

Figure 1 illustrates the overall structure of the morel picking machine. It primarily consists of driving wheels, driven wheels, a mobile platform, a robotic arm rotation mechanism, an upper arm, a lower arm, electric push rods, and a picking claw, among other components. The mobile platform is powered by two DC motors, which allow the machine to move forward and backward during operation. The robotic arm is designed to achieve precise positioning of the picking claw, thereby facilitating the actions of picking, conveying, and collecting.

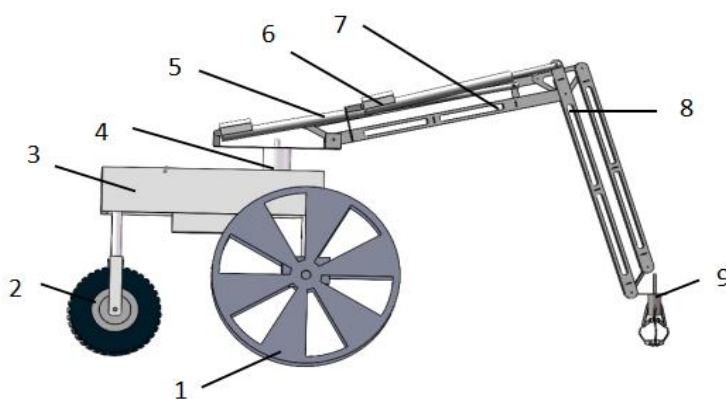


Fig. 1 - Schematic of the morel picking machine

1-driving wheels; 2-driven wheels; 3-mobile platform; 4-robotic arm rotation mechanism; 5-electric push rod for upper arm; 6- electric push rod for lower arm; 7- upper arm; 8- lower arm; 9- picking claw

Working principle of the machine

The machine is operated using a manual remote control. Once the machine is positioned for work, the rotating mechanism of the robotic arm is activated. The electric push rods of both the upper and lower arms facilitate the rotation of the arms, positioning the picking claw over the morels to be harvested. When the fingers of the picking claw close, a blade located at the tips of the fingers severs the stem of the morel, allowing it to be captured by the claw. Subsequently, the electric push rod for the upper arm contracts, elevating the upper arm. Meanwhile, the electric push rod for the lower arm rotates it by a specified angle, positioning the picking claw above the collection box. The fingers of the picking claw then open, depositing the picked morel into the collection box.

Design of the robotic arm

During the picking operation, the movement of the picking claw is simultaneously influenced by the trajectories of both the upper and lower arms (Jun, *et al.*, 2021; Zhang *et al.*, 2015; Zhang, 2019). To further analyse the angular and motion relationships among the upper arm, lower arm, and picking claw, the three-degree-of-freedom robotic arm was simplified, as illustrated in Figure 2 (Zhou, *et al.*, 2012; Yoshida *et al.*, 2022).

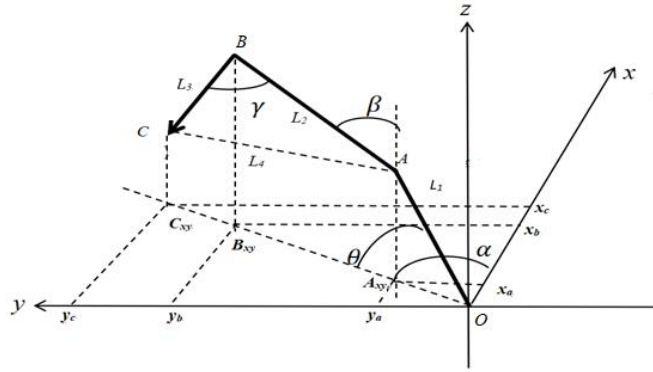


Fig. 2 - Simplified model of the robotic arm

In order to enable the picking claw at the end of the robotic arm to reach the designated picking range, the length of the upper arm was selected to be 800 mm, while the length of the lower arm was set at 650 mm, taking into account the overall structural dimensions of the machine. Using a right-handed coordinate system, the base of the robotic arm coincides with the xOy plane, and the centre of rotation for the robotic arm base is determined as the coordinate origin. The remaining components are arranged on the positive side of each coordinate axis (Zhang et al., 2020). OA represents the robotic arm rotation mechanism mounted on the base, enabling the arm to rotate around the z-axis. The length of OA is 400 mm. AB represents the upper arm, while BC represents the lower arm. θ is the angle between the robotic arm rotation mechanism OA and the xOy plane, α is the angle between the plane in which the robotic arm is situated and the xOz plane, β is the angle between the upper arm AB and the vertical direction, and γ is the angle between the lower arm BC and the upper arm AB.

Based on the geometric relationships illustrated in Figure 2, the following expression can be derived:

$$L_{OC_{xy}} = L_1 \cos \theta + L_2 \sin \beta + L_3 \sin(\gamma - \beta) \tag{1}$$

where:

$L_{OC_{xy}}$ represents the length of the projection of OC onto the xOy plane; L_1 represents the length of OA; L_2 represents the length of AB; L_3 represents the length of BC.

The coordinates of point A can be determined as follows:

$$\begin{cases} x_a = L_1 \cos \theta \cos \alpha \\ y_a = L_1 \cos \theta \sin \alpha \\ z_a = L_1 \sin \theta \end{cases} \tag{2}$$

The coordinates of point C can be expressed as follows:

$$\begin{cases} x_c = [L_1 \cos \theta + L_2 \sin \beta + L_3 \sin(\gamma - \beta)] \cos \alpha \\ y_c = [L_1 \cos \theta + L_2 \sin \beta + L_3 \sin(\gamma - \beta)] \sin \alpha \\ z_c = \sqrt{L_4^2 - (x_c - L_1 \cos \theta \cos \alpha)^2 - (y_c - L_1 \cos \theta \sin \alpha)^2} + L_1 \sin \theta \end{cases} \tag{3}$$

where, L_4 represents the length of AC.

According to the equations presented above, it can be concluded that when θ is 50° , α is 64° , β is 50° , and γ is 80° , the length of OC_{xy} is 1194 mm, which satisfies the requirement for a working radius greater than 1000 mm.

Motion simulation of the robotic arm

The motion trajectory of the robotic arm's end was simulated by importing the robotic arm model into Adams software, as shown in Figure 3.

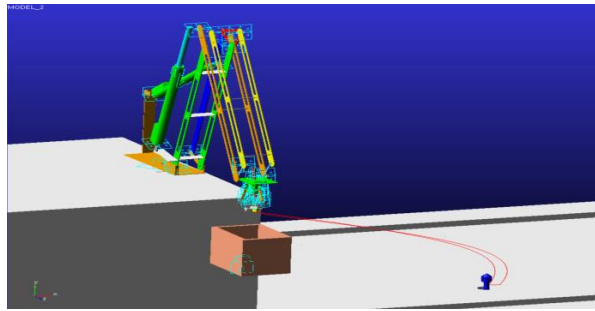


Fig. 3 - Simulation of the motion trajectory of the robotic arm's end

The variation in the mass centre coordinates of the robotic arm's end is shown in Figure 4. The labels "end.CM_Coordinate.X", "end.CM_Coordinate.Y", and "end.CM_Coordinate.Z" represent the coordinates of the centre of mass along the x, y, and z axes respectively. The label "end.CM_Coordinate.Mag" represents the distance from the robotic arm's end to the coordinate origin.

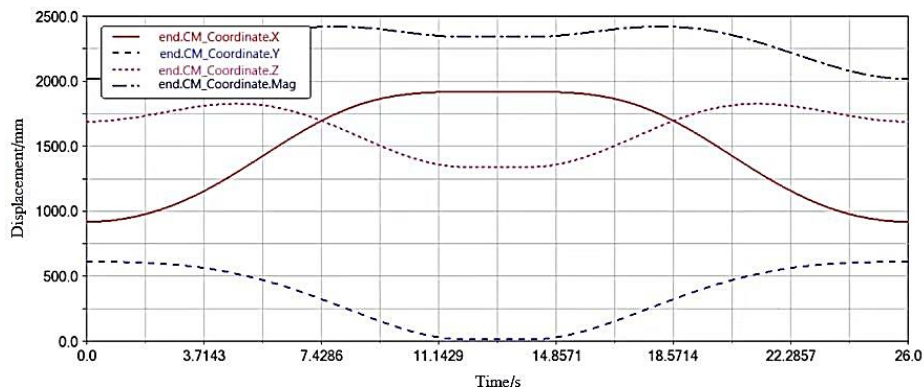


Fig. 4 - Variation in the mass centre coordinates of the robotic arm's end

The robotic arm's end is initially positioned above the collection box, with the y-axis coordinate of its centre of mass at 612.34 mm. Within 12 seconds, the end effector is manoeuvred to the picking position via the robotic arm rotation mechanism, the upper arm, and the lower arm. From 12 to 13 second, the robotic arm remains stationary while performing the picking action. At this moment, the y-axis coordinate of the mass centre of the robotic arm's end is 0.54 mm, indicating that the picking claw is nearly close to the ground. From 13 to 25 second, the robotic arm's end returns to its initial position, completing the collection action.

Force simulation of the robotic arm

An electric push rod with a stroke length of 400 mm and a thrust capacity of 1000 N was selected as the driving unit for the upper arm, while a push rod with the same stroke length of 400 mm and a thrust capacity of 480 N was chosen for the lower arm. The force acted on the robotic arm and the hinges at each connection were analysed using Adams software. Figure 5 illustrates the variation in the support force on the robotic arm. The labels "arm.Support_Force.X", "arm.Support_Force.Y", and "arm.Support_Force.Z" represent the component force along the x, y, and z axes respectively. The label "arm.Support_Force.Mag" represents the resultant force. As shown in Figure 5, the maximum support force reaches 493.76 N at 14 seconds.

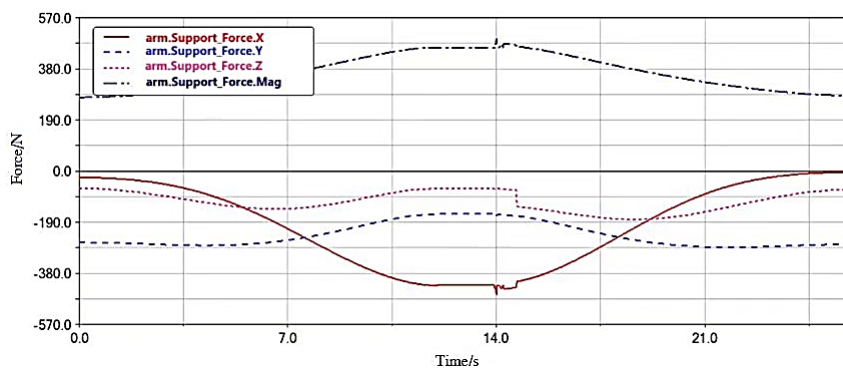


Fig. 5-Variation in the support force on the robotic arm

Figure 6 shows the variation in the force on the hinge connecting the upper arm and the lower arm. The labels “hinge. Force.X”, “hinge. Force.Y” and “hinge. Force.Z” represent the component forces along the x, y, and z axes respectively. The label “hinge.Force.Mag” represents the resultant force. As shown in Figure 6, the resultant force reaches its maximum value of 272.67 N at 26 seconds. The maximum force in the x-axis direction is 65.5 N at 18.2 seconds, the maximum force in the y-axis direction is 264.33 N at 26 seconds, and the maximum force in the z-axis direction is 54.28 N at 4.2 seconds.

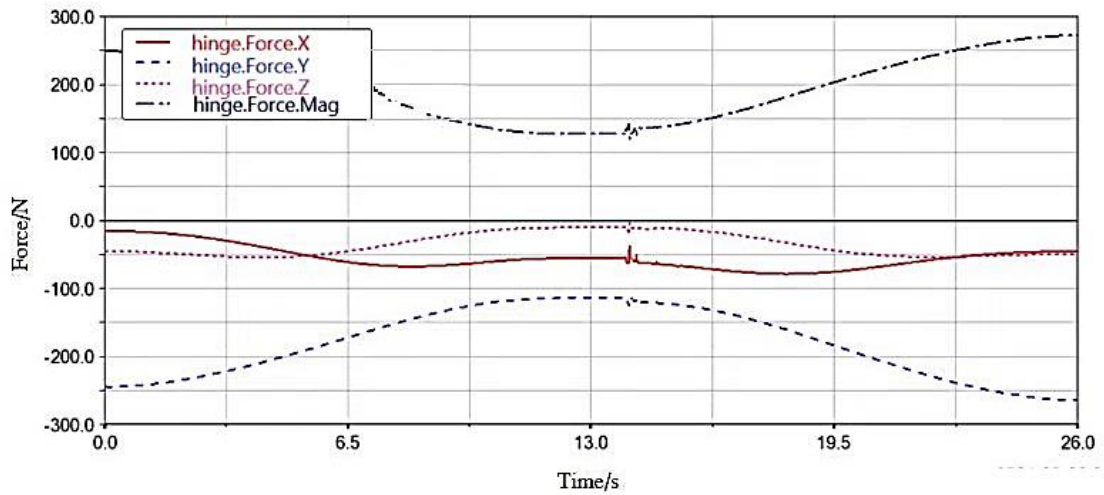


Fig. 6 - Variation in the force on the hinge connecting the upper arm and the lower arm

The robotic arm is constructed from 3 mm low-carbon steel plate. Force analysis indicates that the strength and stiffness of each component meet the necessary requirements. There is no significant deformation during operation, which effectively minimizes shaking and ensures accurate grasping.

Design of the picking claw

When manually picking morels, grasp the stem with the thumb, forefinger, and middle finger, then use a blade to cut it at a specific distance above the ground. This study examines the physical characteristics of morels and simulates the manual harvesting process. Compared to the double-finger structure, the three-finger end effector offers advantages such as high reliability, smooth movement, and resistance to detachment. Although the four-finger structure demonstrates effective grasping capabilities, it is difficult to control, complex in structure, and more expensive (Zhao et al., 2024; Chen et al., 2024). Based on a comprehensive analysis, this study adopts a three-finger structure. The picking claw comprises fingers, links, sliders, and blades, as shown in Figure 7.

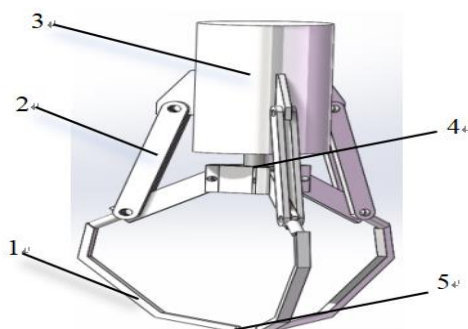


Fig. 7 - Schematic of the picking claw
1-finger; 2-link; 3-frame; 4-slider; 5-blade

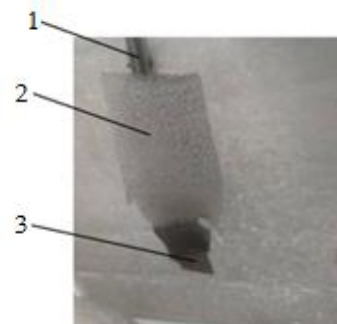


Fig. 8 - Composition of the picking finger
1-finger; 2-elastic foam; 3-blade

The frame of the picking claw is equipped with three fingers arranged uniformly at 120°. A servo motor is utilized to control the movement of these fingers. A power source simultaneously operates the fingers through a wire-pulling mechanism and a four-bar linkage, facilitating both closure and separation. When the servo motor rotates counterclockwise, the contraction of the cable drives the slider upward, causing the fingers to close. Conversely, when the servo rotates clockwise, the cable relaxes, and the fingers separate due to the action of a reset spring.

The reset spring is installed between the frame and the slider, featuring an elasticity coefficient of 1 N/cm, and a stretch of 3 cm. The fingers have a weight of 0.3 kg, while the other components collectively weigh

0.2 kg. The rotation speed of the servo is 120 °/s, and the required servo torque can be calculated to be 15 kg·cm. The selected servo model is the TD-8130MG, which has a torque rating of 29.5 kg·cm, thereby meeting the operational requirements.

The fingers are constructed from 45 steel. To accommodate morels of various sizes and prevent clamping damage, elastic foam was applied to the fingers as a buffer material. A triangular blade with a tip angle of 60 ° was selected and installed at the end of the finger, as illustrated in Figure 8.

The process of picking morels using the fingers was simulated. The variation in fingertip velocity was obtained, as shown in Figure 9. The labels “fingertip.Velocity.X”, “fingertip.Velocity.Y” and “fingertip.Velocity.Z” in the label represent the component velocity along the x, y, and z axes respectively. The label “fingertip.Velocity.Mag” represents the resultant velocity.

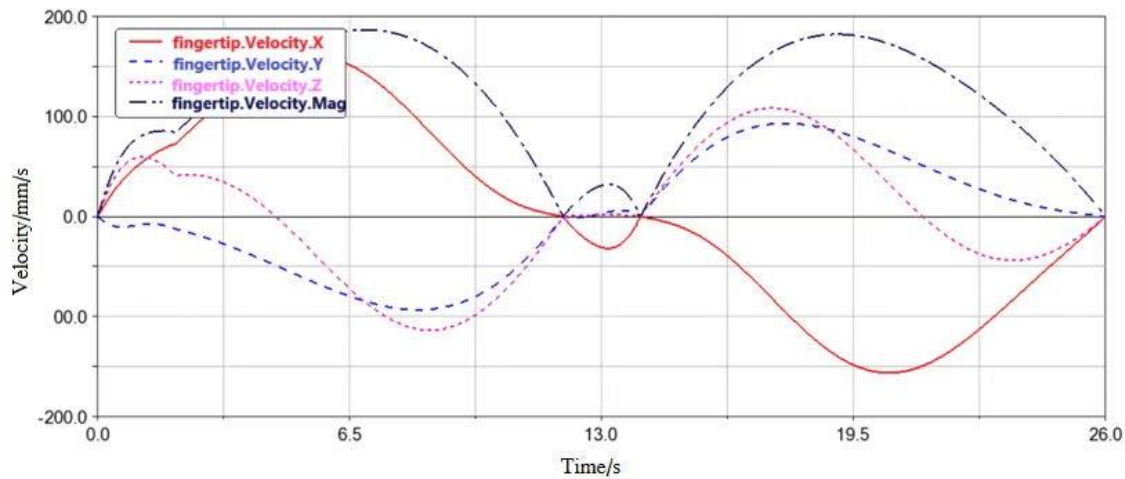


Fig. 9 - Variation in fingertip velocity

From Figure 9, it can be observed that at 12.5 seconds, the picking claw approaches the morel, and the velocity in each coordinate axis direction drops to zero, causing the picking claw to halt at the designated picking position. Between 12.5 and 13 second, the velocities along the y-axis and z-axis of the picking claw remain relatively constant, while the absolute value of the x-axis velocity increases. This indicates that the picking claw is performing a grasping operation on the morel in the x-axis direction. During the interval from 13 to 13.5 seconds, the absolute value of the x-axis velocity decreases, and the picking claw approaches the root of the morel at a reduced velocity for cutting operations. At 13.5 seconds, the velocity drops to zero, signifying the completion of the cutting and grasping actions. Throughout the entire picking process, the velocity of the picking claw changes relatively smoothly, with two brief pauses occurring when approaching the morel and after the cutting is completed. The impact generated by the fingertip is relatively small, which helps to reduce the damage rate of the morel.

Design of the mobile platform

Taking into account the planting environment of morels, the arrangement of all components, and the picking process, the mobile platform was designed to be 1140 mm long, 800 mm wide, and 600 mm high. The platform features a four-wheel support structure, with the front two wheels serving as the driving wheels and the rear two wheels functioning as the driven wheels. A DC motor transmits power through a chain drive to the output shaft, enabling the platform to move forward or backward (Wang et al.,2021). The following formula can be used to calculate the motor power.

$$P_e = \frac{1}{\eta} \left(\frac{mgfv}{3600} + \frac{mgiv}{3600} + \frac{C_d A v^3 m}{76140} + \frac{mga\delta v}{3600} \right) \tag{4}$$

where, P_e represents the motor power, kW; g represents gravitational acceleration, 9.8 N/kg; m represents the full load mass of the mobile platform, 100 kg; f represents the rolling resistance coefficient, 0.6; I represents the ground gradient; A represents the windward area in the forward direction, 1.2 m²; a represents the acceleration of the platform, with a maximum value of 0.5 m/s²; C_d represents the driving resistance coefficient, 0.7; v represents the platform velocity, 3 km/h; η represents the transmission efficiency, 0.9; δ represents the mass conversion coefficient of the platform, 1.2.

When the mobile platform ascends a slope with a gradient of 5% at a constant velocity of 3 km/h, the required motor power is 0.62 kW. When the platform accelerates at a rate of 0.5 m/s², the required motor power is 1.21 kW. Consequently, a brushless DC motor with a power of 1.5 kW was selected.

Prototype experiments

Experiments were carried out at a morel planting facility in Fushun, Liaoning Province, China. The diameter of a mature morel cap ranges from 30 to 60 mm, while the length of the cap varies between 40 and 100 mm. The diameter of the stem measures 20 to 40mm, and the stem length is typically between 50 and 70 mm. The mass of the morel is approximately 15 to 25 g. The experimental site is shown in Figure 10. The purpose of the experiment is to verify whether the robotic arm can accurately position the picking claw to the predetermined picking location, and to determine the optimal length of the blade mounted at the end of the picking finger. A 48V battery served as the power supply for the machine. The control system of the machine consists of a remote control, a receiver, an electronic speed controller, a motor, two electric push rods, and a steering engine. The remote control emits a 2.4GHz signal, which is then received and converted into a PWM (Pulse Width Modulation) signal by the receiver. The electronic speed controller achieves the start, stop, speed regulation of the motor, push rods and steering engine based on the received PWM signal. As a result, the position of the rotating mechanism, the upper arm, the lower arm can be adjusted to realize the picking process. The prototype is illustrated in Figure 11.



Fig. 10 – Experimental site



Fig. 11 – Experimental prototype

The primary factor affecting the picking efficiency is the blade length of the picking claw. If the blade is too short, it becomes challenging to cut the stem; conversely, if the blade is too long, it may inadvertently damage other immature morels. Consequently, four blade length levels were selected: 0 mm, 10 mm, 15 mm, and 20 mm. The index for the experiment included the picking success rate, the damage rate of mature morels, and the damage rate of immature morels. The calculation formulas are as follows:

$$\eta_c = n_c / n \quad (4)$$

$$\eta_d = (n_s + n_a) / n_c \quad (5)$$

$$\eta_z = n_j / n_z \quad (6)$$

where, η_c represents the picking success rate; η_d represents the damage rate of mature morels; η_z represents the damage rate of immature morels; n represents total number of picks; n_c represents the number of successful picks; n_s represents the number of morels with stem damage; n_a represents the number of morels with cap damage; n_j represents the number of damaged immature morels.

RESULTS

During the experiment, 15 mature morels were selected as a group at each level to calculate the experimental index values, with 4 groups being repeated. The damage to the morels caused by mechanical picking is shown in Figure 12.

The picking success rates at different levels are shown in Figure 13. When the picking claw is not equipped with blades, the claw's fingertip is unable to cut through the morel. In this case, the morel is grasped by the picking fingers and extracted from the soil by the robotic arm, leading to a lower success

rate. However, after the installation of the blades, the picking claw can effectively cut the root of the morel, resulting in a significant improvement in the picking success rate. Conversely, if the blade is excessively long, it may cause the picking claw to occupy more workspace, which can hinder smooth grasping movements and lead to a slight decrease in the picking success rate.



Fig. 12 - Morel damage

The damage rates of morels at different levels are shown in Figure 14. When the picking claw is not equipped with blades, the morel tends to break under tension, necessitating that the picking fingers exert additional pressure, which can easily lead to damage. Conversely, after the blades are installed, the morel can be severed with less force, significantly decreasing the damage rate. However, if the blade is excessively long, interference between the blade tips may occur when the claw is closed, potentially increasing the damage rate.

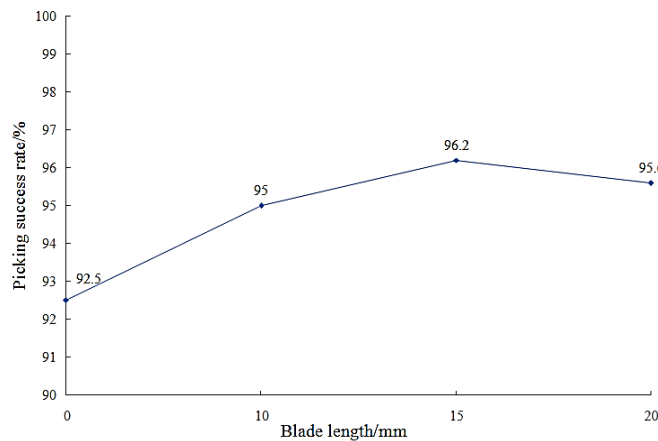


Fig.13 - Picking success rate at different blade lengths

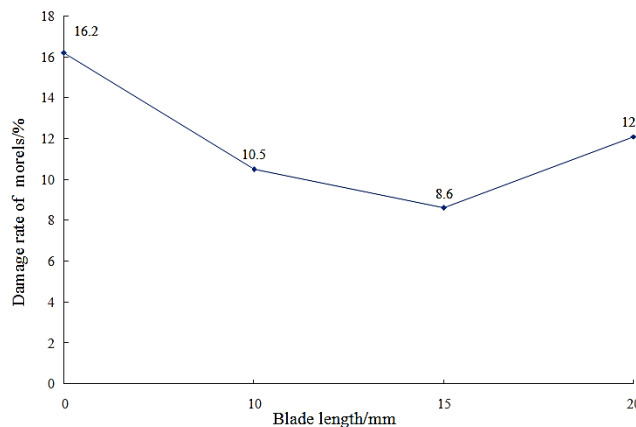


Fig. 14 - Damage rate of morels at different blade lengths

The damage rates of immature morels at different levels are shown in Figure 15. Immature morels are more fragile than mature ones and are typically found near mature morels, making them more susceptible to contact with the picking claw. In the absence of blades, the picking claw lacks sharp edges, which reduces the likelihood of damaging the surrounding immature morels. However, due to the complex and variable picking environment characterized by the irregular distribution of morels and the positional accuracy errors of the robotic arm, the blades are more prone to inadvertently contacting the immature morels during the cutting process, thereby increasing their damage rate.

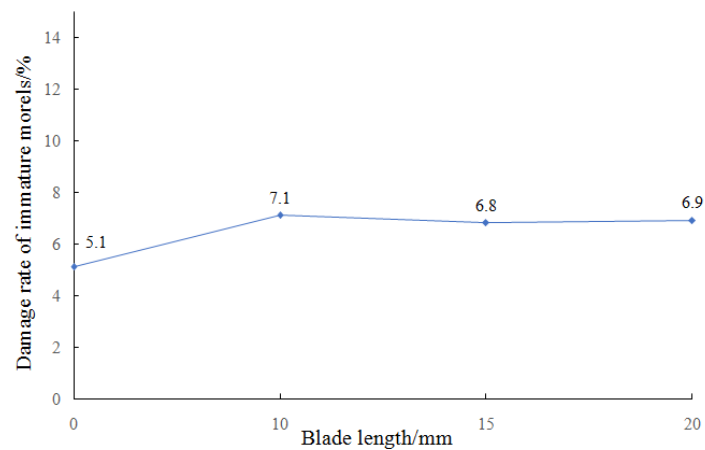


Fig. 15 - Damage rate of immature morels at different blade lengths

According to the experimental data, when the blade length at the end of the picking finger is set to 15 mm, the average picking success rate is 96.2%, the damage rate of morels is 8.6%, and the damage rate of immature morels is 6.8%. The picking machine can effectively grasp morels while maintaining a low damage rate, thereby meeting the requirements for morel picking operations.

CONCLUSIONS

The motion and force of the robotic arm and the picking claw during the picking process were analysed using Adams software. The simulation results proved the correctness of the theoretical model. The robotic arm adopts a three-degree-of-freedom structure, which can achieve precise positioning of the picking claw. The picking machine can perform positioning, cutting, and collection actions within 25 seconds. The picking claw is close to the ground when cutting the morel stem, ensuring the picking quality. The strength and stiffness of each component of the robotic arm meet the necessary requirements, ensuring both motion and grasping accuracy. The picking claw pauses briefly twice: once when approaching the morel and again after cutting. Furthermore, the velocity variation throughout the entire picking process is relatively smooth, which helps minimize damage to the morel.

Through single-factor experiments, the effect of the blade length of the picking finger on the picking success rate, the damage rate of morels, and the damage rate of immature morels was investigated. The results demonstrated that when the blade length was 15 mm, the picking success rate was 96.2%, the damage rate of morels was 8.6%, and the damage rate of immature morels was 6.8%. The picking machine ensures efficient picking operations while minimizing damage to both the picked morels and surrounding immature ones, thereby meeting the requirements for morel picking operations. However, this machine is just a prototype which requires manual operation. In future research, when combined with a visual recognition system for morels, it can work autonomously.

REFERENCES

- [1] Chen, J., Li, H., Liu, L., Jia, J., Zhao, R.; Wu, C. (2024). Design and experimental optimization of split tool type end-effector for picking famous tea (分体刀具式名优茶采摘末端执行器设计与试验优化). *Transactions of the Chinese Society of Agricultural Machinery*, 55(01), 39-46+195.
- [2] Ding, J., Liu, G., Yang, W. (2013). Design and simulation analysis of a fruit picking end-effector (一种果实采摘末端执行器设计与仿真分析). *Journal of Agricultural Mechanization Research*, 5(1), 112-115.
- [3] Gu, B., Ji, C., Wang, H., Tian, G., Zhang, G., Wang, L. (2012). Design and test of intelligent mobile fruit picking robot (智能移动水果采摘机器人设计与试验). *Transactions of the Chinese Society of Agricultural Machinery*, 43(6), 153-160.
- [4] Huang, L., Shang, X., Jiao, S. (2022). Warm-house planting technology of morel mushrooms in Central Plains (中原地区羊肚菌温棚种植技术). *Agricultural Science and Technology Newsletter*, 12(9), 218-221.
- [5] Huang, M., Yang, X., Zhang, C., Li, H., Wu, H., Wang, F. (2023). Study on the picking dynamics of *Agaricus bisporus* and its picking manipulator design (双孢菇采摘动力学研究及其采摘机械手设计). *Journal of Chinese Agricultural Mechanization*, 44 (12), 66-70+98.

- [6] Jun, J., Kim, J., Seol, J., Son, H. I. (2021). Towards an efficient tomato harvesting robot: 3d perception, manipulation, ended-effector. *IEEE Access*, 9,17631-17640.
- [7] Li, G., Ji, C., Zhai, L. (2014), Research progress and analysis of end-effector for fruit and vegetable picking robot (果蔬采摘机器人末端执行器研究进展与分析). *Journal of Chinese Agricultural Mechanization*, 35(5), 231-236+240.
- [8] Liu, W., Zhang, Y., Cai, Y. (2017). Current status and trend of the development of the morel mushroom industry in China (中国羊肚菌产业发展的现状及趋势). *Medicinal Mushroom*, 25(2), 77-83.
- [9] Safeea, M., Neto, P., Bearee, R. (2019). Robot dynamics: A recursive algorithm for efficient calculation of Christoffel symbols. *Mechanism and Machine Theory*, 142, 103589-103589.
- [10] Wang, X., Wu, P., Feng, Q. (2016). Design and test of tomato picking robot system (番茄采摘机器人系统设计及试验). *Journal of Agricultural Mechanization Research*, 38(4), 94-98.
- [11] Wang, X. (2019). *Harvesting tool for morel mushroom (羊肚菌采收工具)*. China, Patent, No.208572865A
- [12] Wang, X., Yuan, S., Shi, Y., Wei, Y., Tao, M. (2021). *A kind of morel mushroom picking and collecting device (一种羊肚菌采摘收集装置)*. China, Patent, No.214628683 A.
- [13] Wang, S. (2021). *A kind of simple morel mushroom harvesting equipment (一种简易羊肚菌采收设备)*. China, Patent, No.215074378 A.
- [14] Wang, C., Wu, W., Liu, J. (2021). Research on motion control system of magnetically guided four rudder wheel heavy-duty AGV (磁导式四舵轮重载 AGV 运动控制系统研究). *Construction Machinery and Equipment*, 52(12), 24-29.
- [15] Yang, Q. (2020). *Research on key technology of target recognition and localization control for flat mushroom picking robot (平菇采摘机器人目标识别与定位控制关键技术研究)*. [Doctoral dissertation, Suzhou University].
- [16] Yoshida, T., Onishi, Y., Kawahara, T., Fukao, T. (2022). Automated harvesting by a dual-arm fruit harvesting robot. *ROBOMECH Journal*, 9:19.
- [17] Yu, H., Zhao, J., Liu, X., Bian E. (2022). *A kind of harvesting tool for morel mushroom (一种羊肚菌采收工具)*. China, Patent, No. 216254377 A.
- [18] Zhao, Q., Huang, Y., Xu, Z., Li, R. (2009). Analysis of the present situation of the cultivation on morels (羊肚菌栽培研究现状). *Journal of Yunnan Agricultural University*, 24(6), 904-907.
- [19] Zhou, Z., Wang, J. (2012). Structural design and parameter optimization of tomato picking robot arm (番茄采摘机器人机械臂结构设计与参数优化). *Anhui Agricultural Science*, 40(22), 11520-11522.
- [20] Zhang, J., Ji, C., Gu, B., Shen, Z., Dong M. (2015), Ontology design of three-degree-of-freedom apple picking robot (三自由度苹果采摘机器人本体设计). *Computer Engineering and Applications*, 51(23), 251-257.
- [21] Zhang, B. (2019). *Research on the control system of Agaricus bisporus picking machine (双孢菇采摘机控制系统研究)*. [Doctoral dissertation, Hebei University of Technology].
- [22] Zhang, J. (2019). *Design of intelligent mushroom picking robot for factorized brown mushroom cultivation (面向工厂化褐菇种植的智能蘑菇采摘机器人设计)*. [Doctoral dissertation, Nanjing Agricultural University].
- [23] Zhang, J., Wang, G., Yuan, X. (2020). A comprehensive evaluation study of design options for omnidirectional mobile robots (全向移动机器人设计方案的综合评价研究). *Mechanical Design and Manufacturing*, (10), 273-275.
- [24] Zhao, X., Zhang, H., Fu, H., Xu, Y., Chen, J. (2024). Design and test of end-effector for picking fresh artichoke peppers (鲜食朝天椒采摘末端执行器的设计与试验). *Transactions of the Chinese Society of Agricultural Machinery*, 10(13), 1-12.